

## Tricritical phenomenon and $H$ - $T$ phase diagram in a single crystal of the double-perovskite iridate $\text{La}_2\text{ZnIrO}_6$

Hui Han,<sup>1,2</sup> Wei Liu,<sup>1,3</sup> Yuhui Dai,<sup>1,3</sup> Yuxia Gao,<sup>4</sup> Zhaoming Tian,<sup>4,\*</sup> Jiyu Fan,<sup>5</sup> Shiming Zhou,<sup>6</sup> Li Pi,<sup>1,6</sup> Changjin Zhang,<sup>1</sup> Lei Zhang,<sup>1,†</sup> and Yuheng Zhang<sup>1,6</sup>

<sup>1</sup>Anhui Key Laboratory of Condensed Matter Physics at Extreme Conditions, High Magnetic Field Laboratory, Chinese Academy of Sciences, Hefei 230031, China

<sup>2</sup>Institute of Physical Science and Information Technology, Anhui University, Hefei 230601, China

<sup>3</sup>University of Science and Technology of China, Hefei 230026, China

<sup>4</sup>Wuhan National High Magnetic Field Center and School of Physics, Huazhong University of Science and Technology, Wuhan 430074, China

<sup>5</sup>Department of Applied Physics, Nanjing University of Aeronautics and Astronautics, Nanjing 210016, China

<sup>6</sup>Hefei National Laboratory for Physical Sciences at the Microscale, University of Science and Technology of China, Hefei 230026, China



(Received 6 May 2018; published 3 August 2018)

We report a detailed study of magnetic properties in double perovskite iridate  $\text{La}_2\text{ZnIrO}_6$  single crystal, which exhibits an antiferromagnetic (AFM) ground state. The field- and angle-dependent magnetizations [ $M(H)$  and  $M(\varphi)$ ] suggest strong magnetic anisotropy in this system. The magnetization of  $\text{La}_2\text{ZnIrO}_6$  is isotropic in the  $ab$  plane, while it is much stronger than that along the  $c$  axis. A field-induced magnetic transition from AFM to ferromagnetic (FM) state is found, which is of a first-order type. The critical behavior is investigated, where critical exponents  $\beta = 0.2317(1)$ ,  $\gamma = 0.9783(2)$ , and  $\delta = 5.0071(5)$  are obtained. The critical exponents belong to the universality class of the tricritical mean-field model, which indicates a field-induced tricritical phenomenon. Based on the scaling equations, we construct the  $H$ - $T$  phase diagram for  $\text{La}_2\text{ZnIrO}_6$  single crystal with  $H//b$ . A tricritical point is revealed at the intersection point between the AFM, FM, and paramagnetic phases ( $T_{tr} \approx 8$  K;  $H_{tr} \approx 170$  Oe).

DOI: [10.1103/PhysRevB.98.054403](https://doi.org/10.1103/PhysRevB.98.054403)

### I. INTRODUCTION

Iridates represent unique materials with a delicate balance of spin-orbital coupling and electron correlation, which exhibit exotic quantum phases such as the  $J_{\text{eff}} = 1/2$  Mott insulators [1–4], quantum spin liquids [5–7], field-induced quantum transitions [8,9], topological Mott insulators [10–12], and Weyl semimetals [13]. These attractive physical phenomena result from the interplay between the spin-orbital coupling ( $\lambda$ ), Coulomb repulsion ( $U$ ), Hund's coupling ( $J_H$ ), and crystal field splitting ( $\Delta_{CF}$ ), which involves coupling between the charge, orbit, spin, and lattice degrees of freedom [14]. Among iridates, the double perovskite  $A_2B\text{IrO}_6$  ( $A$  = rare earth or alkaline earth element and  $B = 3d$  transition metal element) is one of the most prominent systems, in which some emergent physical behaviors have been reported [15]. Its structure is a monoclinic deformation belonging to the space group  $P2_1/n$ , where the B and Ir ions alternately occupy two interpenetrating face-centered-cubic (fcc) sublattices [16]. These materials exhibit diverse magnetic ground states, such as noncollinear antiferromagnetism induced by strong coupled Cu ( $S = 1/2$ ) and Ir ( $J = 1/2$ ) in  $\text{La}_2\text{CuIrO}_6$  [17], covalency and spin-orbital coupling driven magnetism in  $\text{Sr}_2\text{CaIrO}_6$  and  $\text{Sr}_2\text{MgIrO}_6$  [18], diluted localized paramagnetic moments in nonmagnetic  $\text{Ba}_2\text{YIrO}_6$  [19], canted antiferromagnetic (AFM)

order in  $3d$ - $5d$  coupled  $\text{La}_2\text{CoIrO}_6$  [20,21], and possible half-metallic antiferromagnetism in Sr-doped  $\text{Pr}_2\text{MgIrO}_6$  [22].

In the double perovskite iridates,  $\text{La}_2\text{M}\text{IrO}_6$  ( $B = \text{Zn}$  and  $\text{Mg}$ ) are distinct prototypical systems as geometrical frustrated  $J_{\text{eff}} = 1/2$  Mott insulators [23]. Studies have indicated that both  $\text{La}_2\text{ZnIrO}_6$  and  $\text{La}_2\text{MgIrO}_6$  exhibit  $A$ -type AFM ground states at low temperature, where the moments of Ir are ferromagnetically aligned within single layered  $ab$  plane but staked antiferromagnetically along the  $c$  axis [23,24]. However, different from  $\text{La}_2\text{MgIrO}_6$ , the  $A$ -type AFM ordered moments in  $\text{La}_2\text{ZnIrO}_6$  are canted. Therefore, a weak ferromagnetic (FM) characteristic has been observed [25,26], implying that multiple interplays and competitions cause more complex magnetic behaviors in  $\text{La}_2\text{ZnIrO}_6$ .

Although many investigations have been performed on  $\text{La}_2\text{ZnIrO}_6$  to clarify its physical properties, complete understanding of this system remains unclear. Moreover, to our knowledge, previous experimental studies on  $\text{La}_2\text{ZnIrO}_6$  are only confined to polycrystalline samples instead of single crystal. Therefore, some important properties, such as crystal and magnetic anisotropy, are impossible to accurately determine. In order to solve these questions thoroughly, a single crystal  $\text{La}_2\text{ZnIrO}_6$  with high quality has been chosen to be studied in this work. Based on the measurement of magnetization along the different directions, we find single crystal  $\text{La}_2\text{ZnIrO}_6$  presents an excellent isotropy within the  $ab$  plane but shows a strong anisotropy between the  $ab$  plane and  $c$  axis. Meanwhile, a field-induced magnetic phase transition from AFM to FM is observed, which is of a first-order type.

\*Corresponding author: tianzhaoming@hust.edu.cn

†Corresponding author: zhanglei@hmf.ac.cn

The critical exponents  $\beta$ ,  $\gamma$ , and  $\delta$  are deduced, which suggest a field-induced tricritical phenomenon in  $\text{La}_2\text{ZnIrO}_6$ . Based on the scaling equations, the  $H$ - $T$  phase diagram is constructed, where a tricritical point is revealed at the intersection point between the AFM, FM, and paramagnetic (PM) phases.

## II. EXPERIMENTAL METHODS

Single crystals of  $\text{La}_2\text{ZnIrO}_6$  were grown by the KF flux method. A polycrystalline sample of  $\text{La}_2\text{ZnIrO}_6$  was first prepared by the solid state reaction using stoichiometric starting materials  $\text{La}_2\text{O}_3$  (99.9%, Alfa Aesar) and  $\text{IrO}_2$  (99.9%). Then, single crystals were grown by combining the polycrystalline sample with KF flux in a ratio of 1 : 300. After being heated to 1100 °C and annealed for 5 h, the as-grown sample was slowly cooled down to 850 °C at a rate of 2 °C/h. The single crystals were obtained from the flux by dissolving the flux in water.

The chemical compositions were carefully checked by the energy dispersive x-ray (EDX) spectrometry. The crystal structure and orientations were determined by the Rigaku Gemini S Ultra four-circle single crystal x-ray diffractometer (XRD) (see Supplemental Material for details [27]). The magnetization was measured using a quantum design vibrating sample magnetometer (SQUID-VSM). The no-overshoot mode was applied to ensure a precise magnetic field. The magnetic field was relaxed for two minutes before data collection. For the measurement of initial isothermal magnetization, the sample was first heated adequately above the phase transition temperature for 10 min, then cooled to the target temperature under zero magnetic field.

## III. RESULTS AND DISCUSSION

Figure 1(a) shows the crystal structure of  $\text{La}_2\text{ZnIrO}_6$ . The double perovskite cells are separated by LaO layers, where

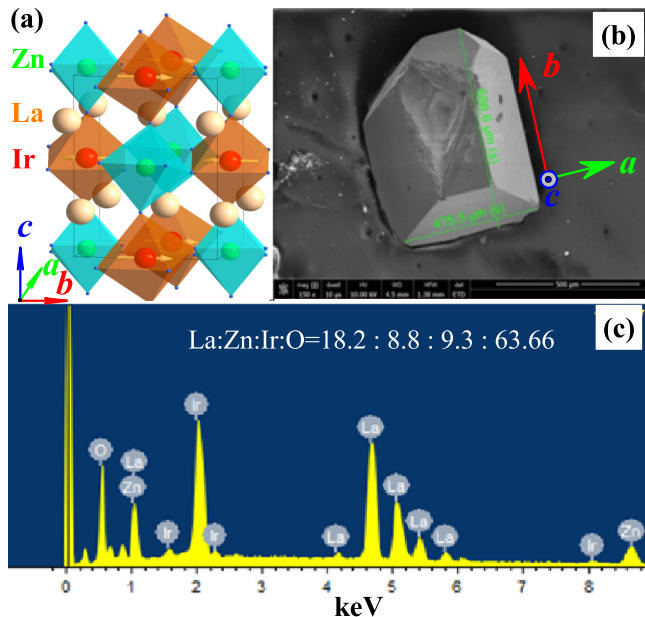


FIG. 1. (a) Unit cell of double perovskite  $\text{La}_2\text{ZnIrO}_6$ ; (b) the morphology of the single crystal; (c) the EDX spectrum for the single crystal.

Ir and Zn alternatively locate in the octahedrons formed by  $\text{O}_6$ . Due to the lattice distortion, the  $\text{IrO}_6$  octahedrons are rotated. Figure 1(b) depicts the morphology of the  $\text{La}_2\text{ZnIrO}_6$  single crystal utilized in the present investigation. The crystal orientations of the single crystal are determined by the four-circle single crystal XRD, as marked in Fig. 1(b). The lattice constants are determined as  $a = 5.550(5)$  Å,  $b = 5.717(6)$  Å, and  $c = 7.930(9)$  Å, which are in agreement with the previous report [16]. The EDX spectrum gives the typical chemical proportion of La : Zn : Ir : O = 18.2 : 8.8 : 9.3 : 63.66, which is very close to the expected chemical proportion of  $\text{La}_2\text{ZnIrO}_6$ . All of these results indicate that the  $\text{La}_2\text{ZnIrO}_6$  single crystal studied here is of high quality.

Figure 2(a) depicts the temperature dependence of magnetization  $[M(T)]$  under applied field  $H = 200$  Oe. The external field  $H$  is applied parallel to the  $b$  axis ( $H//b$ ) and  $c$  axis ( $H//c$ ), respectively. The  $M(T)$  curve with  $H//a$  is not shown here because it is the same as that with  $H//b$ . All  $M(T)$  curves are collected on warming under sequences of zero-field cooling (ZFC) and field cooling (FC), respectively.

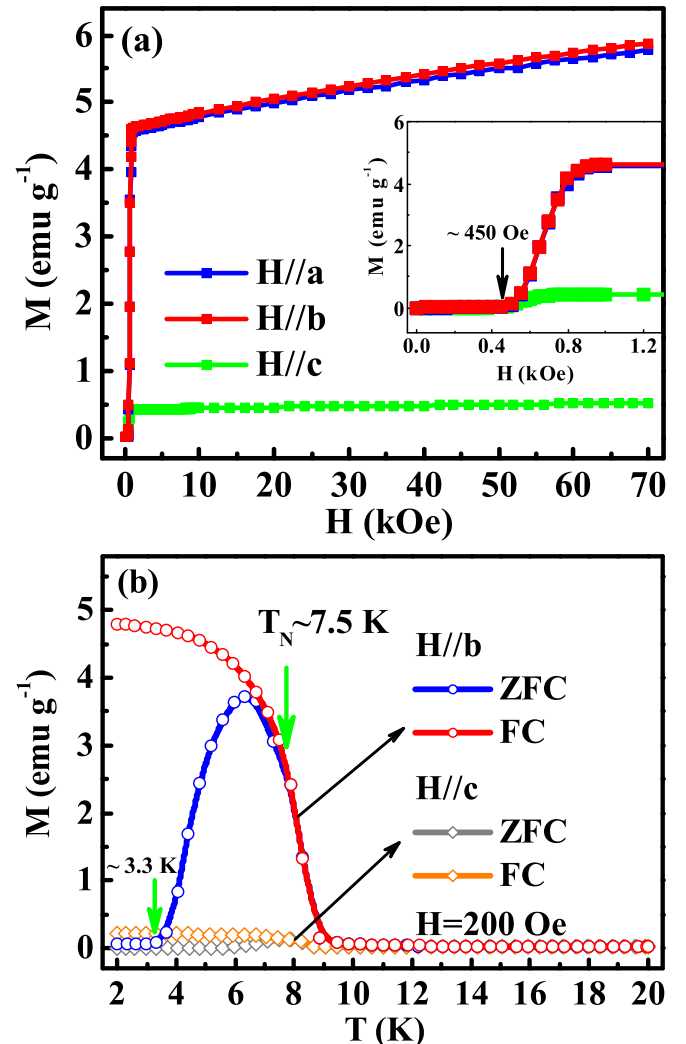


FIG. 2. (a) Temperature dependence of magnetization  $[M(T)]$  under  $H = 200$  Oe with  $H//b$  and  $H//c$ ; (b) the initial isothermal magnetization at  $T = 2$  K  $[M(H)]$  with  $H//a$ ,  $H//b$ , and  $H//c$ .

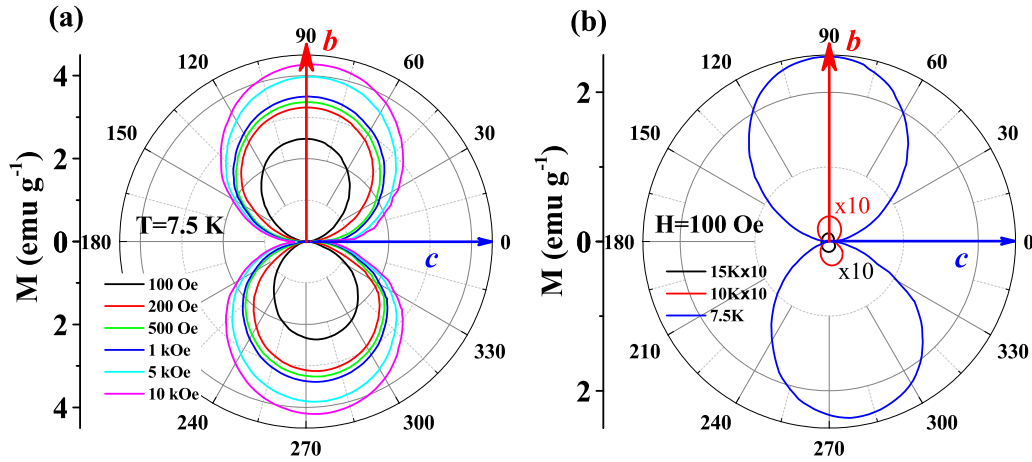


FIG. 3. Angle dependence of magnetization [ $M(\varphi)$ ]: (a)  $M(\varphi)$  at  $T = 7.5$  K under selected fields; (b)  $M(\varphi)$  at selected temperature with  $H = 100$  Oe.

When  $H//b$ ,  $M(T)$  curves exhibit an obvious magnetic phase transition at  $T_N \sim 7.5$  K, which is consistent with the previous reports [25,26]. Below  $T_N$ , a bifurcation occurs to  $M(T)$  curves under ZFC and FC. For the  $M(T)$  curve under ZFC, the magnetization abruptly decreases below  $T_N$  with the decrease of temperature, and almost reaches zero value at  $T \sim 3.3$  K. The  $M(T)$  behavior under ZFC shows a typical AFM phase transition, where the decrease of  $M$  is due to the AFM ordering of moments. Different from the  $M(T)$  under ZFC, the  $M(T)$  curve under FC keeps a continuous increase with the decrease of temperature to the lowest temperature. When the field is applied along the  $c$  axis, the magnetization values are much smaller compared with those with  $H//b$ . In addition, the phase transition on the  $M(T)$  curves with  $H//c$  is very vague. The  $M(T)$  and  $M(H)$  behaviors indicate that the magnetization of  $\text{La}_2\text{ZnIrO}_6$  exhibits strong anisotropy between  $a(b)$  axis and  $c$  axis.

Figure 2(b) plots the initial isothermal magnetization [ $M(H)$ ] with  $H//a$ ,  $H//b$ , and  $H//c$  at  $T = 2$  K for  $\text{La}_2\text{ZnIrO}_6$ . The  $M(H)$  curve with  $H//a$  coincides with that with  $H//b$ , indicating that  $a$  and  $b$  axis are equivalent in magnetism. Namely, the magnetic properties are isotropic in the  $ab$  plane. Moreover, both  $M(H)$  curves with  $H//a$  and  $H//b$  show large magnetization. On the contrary, for  $H//c$ , the  $M(H)$  remains a small value even when  $H$  reaches 7 T. The  $M(H)$  curves with  $H//a(b)$  present an obvious magnetic ordering behavior, while it is vague for that with  $H//c$ . As we know,  $\text{La}_2\text{ZnIrO}_6$  exhibits an  $A$ -type AFM ground state as shown in Fig. 1(a), where the moments are ferromagnetically within the single layered  $ab$  plane while stacked antiferromagnetically along the  $c$  axis [23,24]. The different behaviors of the  $M(H)$  curves with  $H//a(b)$  and  $H//c$  imply that the AFM ordering along the  $c$  axis is very strong and difficult to break by the external magnetic field. The inset of Fig. 2(a) depicts the detailed variation of  $M(H)$  in low field region. A platform is found below  $H \sim 450$  Oe. As  $H > 450$  Oe, the magnetization of  $H//a(b)$  shows a rapid increase. This result means the AFM coupling between two adjoining  $ab$  planes is very weak, because a quite small field of 450 Oe can transfer the magnetic coupling from AFM to

FM, which gives a large increase to the magnetization with  $H//a(b)$  in Fig. 2(b).

For further understanding of the magnetic anisotropy in  $\text{La}_2\text{ZnIrO}_6$ , the angle dependence of magnetization [ $M(\varphi)$ ] is performed, as displayed in Fig. 3. Figure 3(a) shows the  $M(\varphi)$  curves at  $T = 7.5$  K under selected fields. The  $M(\varphi)$  curves are measured from the  $c$  axis to the  $b$  axis, where  $\varphi$  is defined as the angle between the external field  $H$  and the  $c$  axis. With the change of  $\varphi$ ,  $M$  value is the minimum when  $H//c$ , while it reaches the maximum when  $H//b$ . Figure 3(b) presents  $M(\varphi)$  curves under fixed  $H = 100$  Oe at different temperatures. The  $M(\varphi)$  values at  $T = 10$  K and 15 K are much smaller than that at  $T = 7.5$  K. The  $M(\varphi)$  curve at  $T = 10$  K still exhibits magnetic anisotropy (the  $M$  at 10 K has been magnified 10 times for clarity), which may be due to the strong magnetic fluctuation near the magnetic phase transition. The  $M(\varphi)$  curve at  $T = 15$  K does not display magnetic anisotropy. The  $M(\varphi)$  curves indicate that single crystal  $\text{La}_2\text{ZnIrO}_6$  exhibits strong magnetic anisotropy below  $T_N$ , which is determined by the  $A$ -type AFM ordering characteristic in  $\text{La}_2\text{ZnIrO}_6$ .

As can be seen, platforms emerge on the  $M(H)$  and  $M(T)$  curves in low field and low temperature regions, which should be deeply investigated. Figure 4(a) gives the magnified isothermal  $M(H)$  curves in the low field region with  $H//b$  at  $T = 2$  K and 7.5 K, and the inset of Fig. 4(a) shows the whole  $M(H)$  curves. As expected, a platform appears on the initial  $M(H)$  curve with  $H//b$  at  $T = 2$  K in low field region, which suggests an AFM ground state. With the increase of  $H$ ,  $M$  increases rapidly when  $H$  exceeds  $H_{AF}^1 \sim 400$  Oe [ $H_{AF}^1$  is the critical field at the abruptly increasing point on the initial  $M(H)$  curve, as marked in Fig. 4(a)]. Finally,  $M$  reaches the saturated value at  $H_S \sim 800$  Oe ( $H_S$  is the saturation field). However, this platform is not observed on the  $M(H)$  curve at  $T = 7.5$  K. The change of the  $M(H)$  behavior with the applied field suggests a field-induced magnetic transition in  $\text{La}_2\text{ZnIrO}_6$ . In order to investigate this platform and magnetic phase transition, the initial  $M(H)$  curves in the low field region at different temperatures range from 2 K to 10 K with  $H//b$  displayed in Fig. 4(b). Below  $T \sim 7$  K, each initial  $M(H)$  curve exhibits a platform below  $H_{AF}^1$ , and

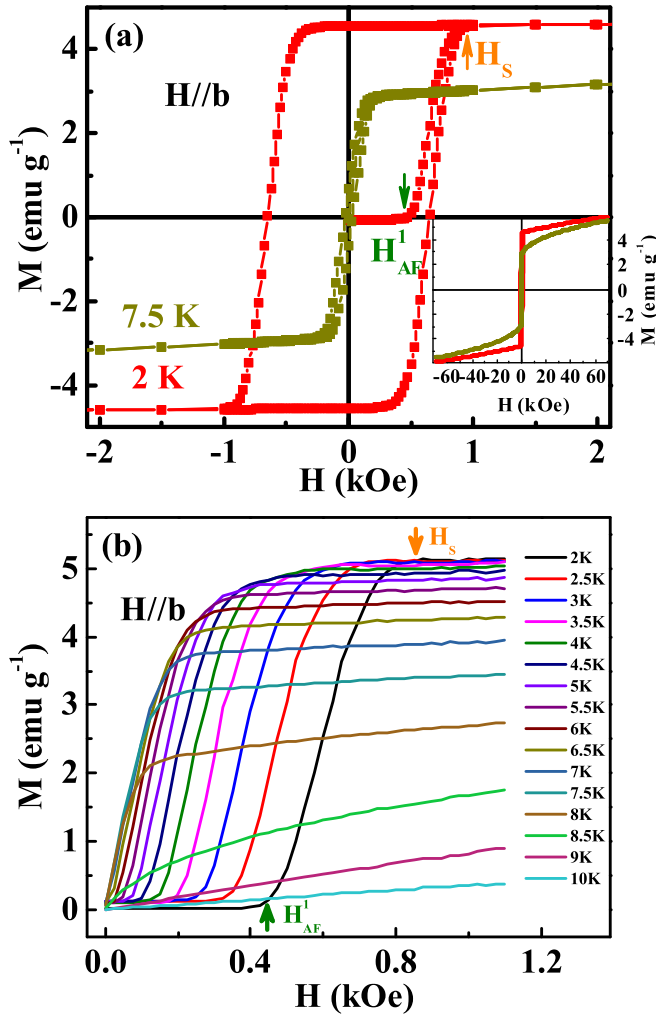


FIG. 4. (a)  $M(H)$  curves with  $H//b$  at 2 K and 7.5 K [the inset shows whole  $M(H)$ ]; (b) the initial  $M(H)$  curves with  $H//b$  at temperature range from 2 K to 10 K ( $H_{AF}^1$  and  $H_S$  indicate the critical fields of AFM and FM transition, respectively).

reaches the saturation at  $H_S$ . However, the platform shrinks when the temperature increases, leading to the decrease of  $H_{AF}^1$  with the increase of temperature. The platform finally disappears on the initial  $M(H)$  curve when  $T > 7$  K, where the initial  $M(H)$  curves show a rapid increase once the magnetic field is applied. As we know, the  $\text{La}_2\text{ZnIrO}_6$  exhibits an A-type AFM ground state below  $T_N \sim 7.5$  K. The initial  $M(H)$  curves in Fig. 4(b) show that a platform caused by the A-type AFM ground state can be destroyed by the applied magnetic field along the  $b$  axis. When the A-type AFM ground state is destroyed by the  $H$  along  $b$  axis, it evolves into a canted AFM phase, which causes the rapidly increasing region on initial  $M(H)$  curves. Further increasing the magnetic field, the canted AFM changes into an FM phase when  $H$  exceeds  $H_S$ .

The study of the magnetization shows that the single crystal  $\text{La}_2\text{ZnIrO}_6$  exhibits an FM characteristic in the high field region when  $H//b$ . For an FM phase transition, the investigation of critical behavior of the phase transition is an effective means to disclose the magnetic interactions. Figure 5(a) plots the initial  $M(H)$  with  $H//b$  at selected temperature around the

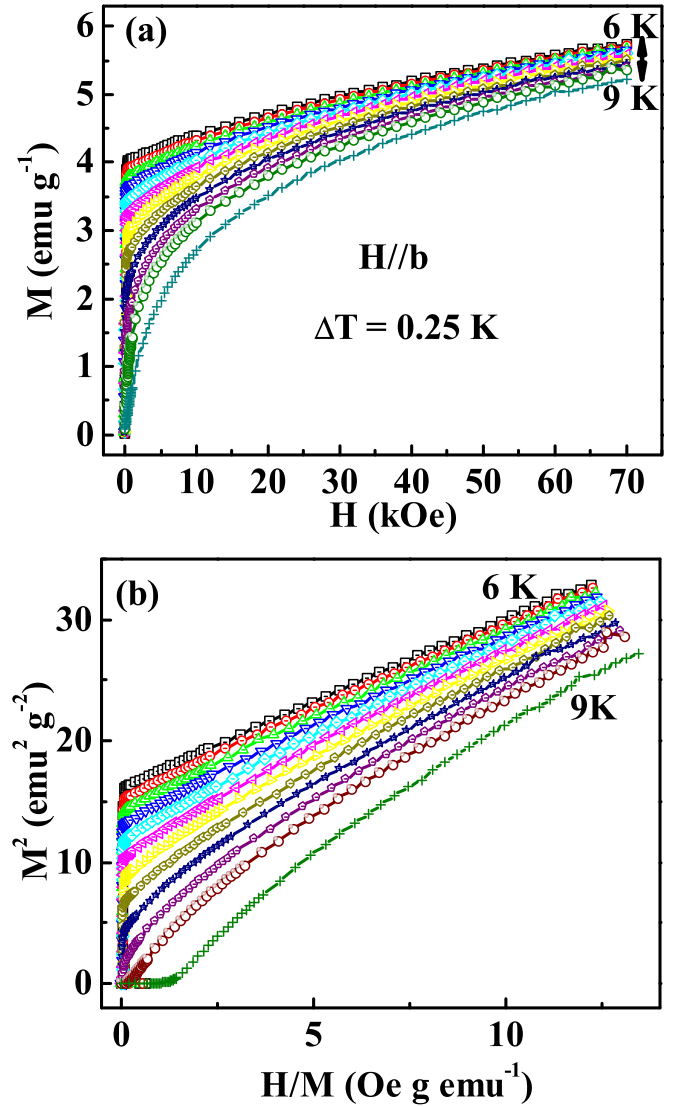


FIG. 5. (a) Initial isothermal  $M(H)$  around the critical temperature  $T_C$  with  $H//b$ ; (b) the Arrott plot of  $M^2$  vs  $H/M$  for  $\text{La}_2\text{ZnIrO}_6$ .

phase transition temperature. Generally, the phase transition can be roughly judged by the Arrott plot. Figure 5(b) gives the Arrott plot of  $M^2$  vs  $H/M$  based on the initial  $M(H)$  curves [28]. The  $M^2$  vs  $H/M$  curves for  $\text{La}_2\text{ZnIrO}_6$  exhibit quasistraight lines in the high field region. However, these lines are not parallel to each other, which indicates that the Landau mean field model is invalid for  $\text{La}_2\text{ZnIrO}_6$ . More universally,  $M(H)$  curves at the vicinity of the phase transition follow the Arrott-Noakes equation of state [29]:

$$(H/M)^{1/\gamma} = (T - T_C)/T_C + (M/M_1)^{1/\beta}, \quad (1)$$

where  $M_1$  is a constant and  $\gamma$  and  $\beta$  are critical exponents. Furthermore, in the vicinity of the magnetic phase transition, these critical exponents are determined by a series of functions [30,31]:

$$M_S(T) = M_0(-\varepsilon)^\beta, \quad \varepsilon < 0, \quad T < T_C, \quad (2)$$

$$\chi_0^{-1}(T) = (h_0/M_0)\varepsilon^\gamma, \quad \varepsilon > 0, \quad T > T_C, \quad (3)$$

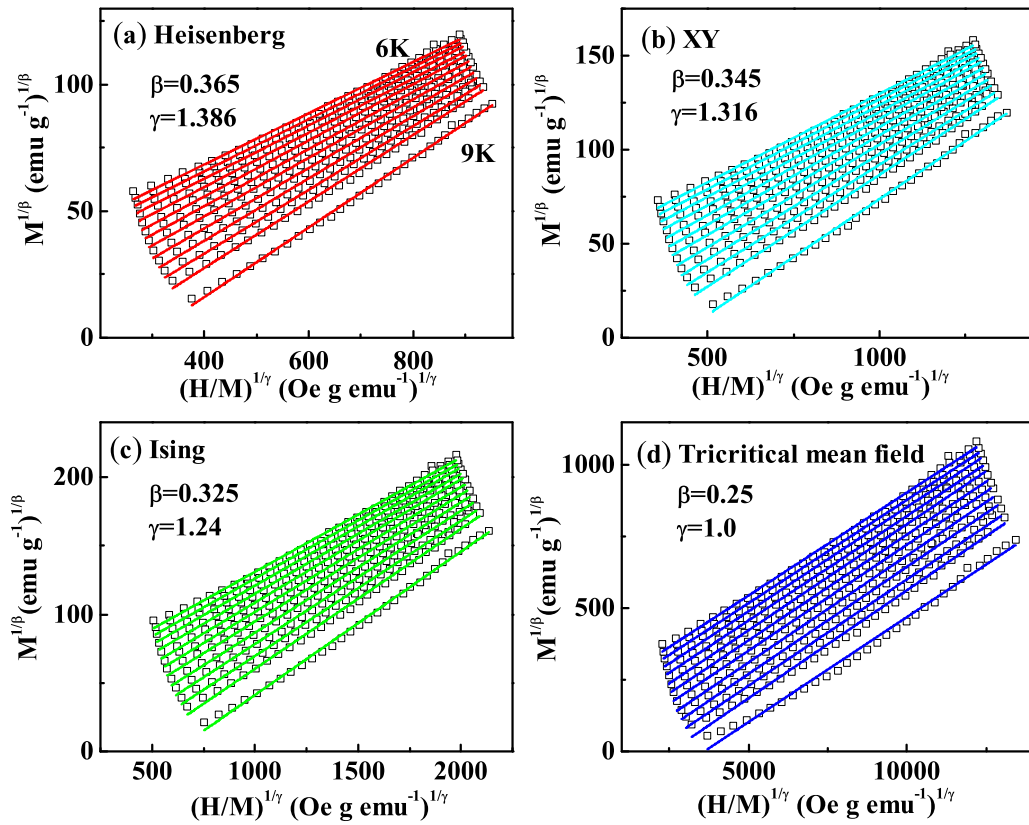


FIG. 6. Isotherms of  $M^{1/\beta}$  vs  $(H/M)^{1/\gamma}$  fitted by lines with parameters of (a) Heisenberg model (red), (b)  $XY$  model (cyan), (c) Ising model (green), and (d) tricritical mean-field model (blue).

where  $M_S$  is the spontaneous magnetization,  $\chi_0$  is initial susceptibility, and  $\varepsilon = (T - T_C)/T_C$  is the reduced temperature;  $M_0/h_0$  is critical amplitude. The critical exponent  $\beta$  is associated with  $M_S$  and  $\gamma$  is responding to  $\chi_0$ . The relation of  $M^{1/\beta}$  vs  $(H/M)^{1/\gamma}$  forms the modified Arrott plot, which should consist of a series of parallel straight lines.

As we know, the magnetic interaction can be classified based on the spin-dimensionality  $n$  [31]. When  $n = 3$ , the spin interaction belongs to the Heisenberg model, which indicates an isotropic magnetic coupling. When  $n = 2$ , it suggests a two-dimensional spin interaction geared to the  $XY$  model. When  $n = 1$ , the spin interaction belongs to the Ising model, indicating an anisotropic magnetic interaction [31]. In a system with multiple phases, a tricritical phenomenon may occur, where a tricritical point (TCP) could be found at the intersection point [32]. Due to the three-dimensional structural characteristic of fcc lattice, the spatial dimensionality ( $d$ ) is considered as  $d = 3$ . Therefore, three models consisting of Heisenberg model ( $\beta = 0.365$ ,  $\gamma = 1.386$ ),  $XY$  model ( $\beta = 0.345$ ,  $\gamma = 1.316$ ), and Ising model ( $\beta = 0.325$ ,  $\gamma = 1.24$ ) with  $n$  ranging from 3 to 1, as well as the tricritical mean-field model ( $\beta = 0.25$ ,  $\gamma = 1.0$ ), are utilized to construct the tried modified Arrott plots [32,33]. The tried modified Arrott plots based on different theoretical models are shown in Figs. 6(a), 6(b) 6(c), and 6(d), respectively. There are two criteria to determine the best model: (1) the line should be straight and (2) they should be parallel to each other. According to Eq. (1),  $M^{1/\beta}$  vs  $(H/M)^{1/\gamma}$  should exhibit a series of straight lines parallel to each other with the same slope [ $S(T)$ ] around the

critical temperature. All these four models present straight lines in the high field region. Actually, the best model can be distinguished clearly by the normalized slope ( $NS$ ) which is defined by  $NS = S(T)/S(T_C)$  [where  $S(T)$  is the slope of  $M^{1/\beta}$  vs  $(H/M)^{1/\gamma}$ , and  $S(T_C)$  is that at  $T_C$ ] [34]. For a most satisfied model, all  $NS$  values should approach “1” closely. Figure 7 plots the temperature dependence of  $NS$  for the four tried modified Arrott plots, which display that the  $NS$  of the tricritical mean-field model is close to 1 mostly. This result indicates that the tricritical mean-field model is the best one to describe the critical behavior of  $\text{La}_2\text{ZnIrO}_6$ .

Based on the tried modified Arrott plot,  $\beta$  and  $\gamma$  can be obtained by the iteration method [35]. The linear extrapolation of  $M^{1/\beta}$  vs  $(H/M)^{1/\gamma}$  line from the high field region to the intercepts with the axes  $M^{1/\beta}$  and  $(H/M)^{1/\gamma}$  yields  $M_S(T, 0)$  and  $\chi_0^{-1}(T, 0)$  under zero field. The critical exponents can be obtained by fitting the temperature dependence of  $M_S$  and  $\chi_0^{-1}$ , as depicted in Fig. 8(a). Subsequently,  $\beta = 0.2317(1)$  with the critical temperature  $T_C = 7.35(6)$  K and  $\gamma = 0.9783(2)$  with  $T_C = 7.39(2)$  K are obtained for  $\text{La}_2\text{ZnIrO}_6$ .

In addition, the critical exponent  $\delta$ , which is associated with the critical temperature  $T_C$ , can be obtained from the initial  $M(H)$  at  $T_C$  as [30,31]

$$M = DH^{1/\delta}, \quad \varepsilon = 0, \quad T = T_C, \quad (4)$$

where  $D$  is the critical amplitude. Based on Eq. (4), there is  $\log(M) = \log(D) + 1/\delta \log(H)$ . Thus  $1/\delta$  can be obtained by the linear fitting of  $\log(M)$  vs  $\log(H)$ . Figure 8(b) shows the critical initial  $M(H)$  at  $T_C = 7.5$  K on log-log scale,

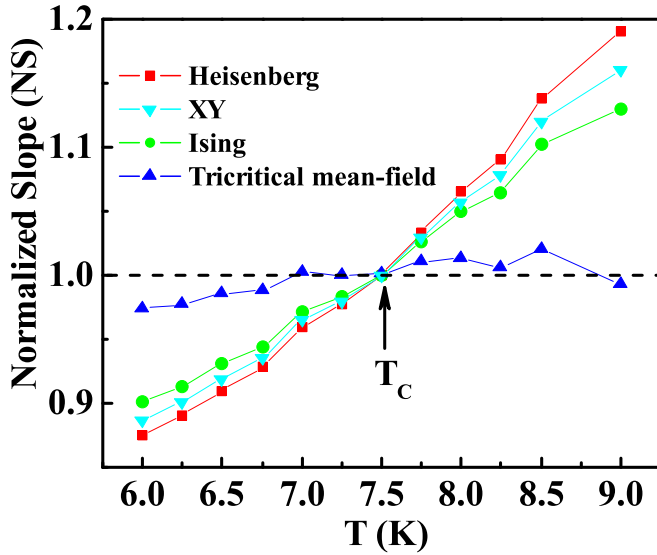


FIG. 7. Temperature dependence of normalized slope ( $NS$ ) for the four theoretical models.

which gives  $\delta = 5.0071(5)$  in the high field region ( $H > H_S$ ). The self-consistency of the obtained critical exponents can be testified by Widom scaling law [36]:

$$\delta = 1 + \frac{\gamma}{\beta}. \quad (5)$$

According to the Widom scaling law,  $\delta = 5.2221(7)$  is calculated, which is close to that obtained from the experimental critical isothermal analysis. The self-consistency confirms the reliability of the obtained critical exponents.

The obtained critical exponents [ $\beta = 0.2317(1)$ ,  $\gamma = 0.9783(2)$ ,  $\delta = 5.0071(5)$ ] are consistent with the theoretical prediction of the tricritical mean-field model ( $\beta = 0.25$ ,  $\gamma = 1.0$ ,  $\delta = 5.0$ ), which suggests a field-induced tricritical phenomenon in  $\text{La}_2\text{ZnIrO}_6$ . The tricritical phenomenon usually occurs at the boundary between the first-order and the second-order phase transitions [37]. In the perovskite manganite, the tricritical phenomenon can be induced by the doping effect, such as  $\text{La}_{0.1}\text{Nd}_{0.6}\text{Sr}_{0.3}\text{MnO}_3$ ,  $\text{La}_{0.6}\text{Ca}_{0.4}\text{MnO}_3$ , and  $\text{La}_{0.7}\text{Ca}_{0.2}\text{Sr}_{0.1}\text{MnO}_3$  [34,38,39]. In these perovskite manganites, the doping suppresses the first-order phase transition into a second-order one, where the tricritical phenomenon occurs when the first-order phase transition just is suppressed by the doping. Other means, such as magnetic field and pressure, can also induce a tricritical phenomenon [37]. In  $\text{MnSi}$ , both the external field and pressure can suppress the first-order transition into a second-order one, where a tricritical critical phenomenon is found [40–43]. Recently, a high magnetic field induced tricritical phenomenon is found in the  $\text{USb}_2$ , which also exhibits an AFM ground state [44].

Since the tricritical phenomenon usually occurs in a system with multiple and complex phases, it is necessary to construct the phase diagram. Our recent study shows that the scaling of the magnetization curves is an effective method to construct the phase diagram [45]. Based on the critical exponents,  $M(H)$  curves should follow the scaling equations. Defining the renormalized magnetization ( $m$ ) as  $m \equiv \varepsilon^{-\beta} M(H, \varepsilon)$  and

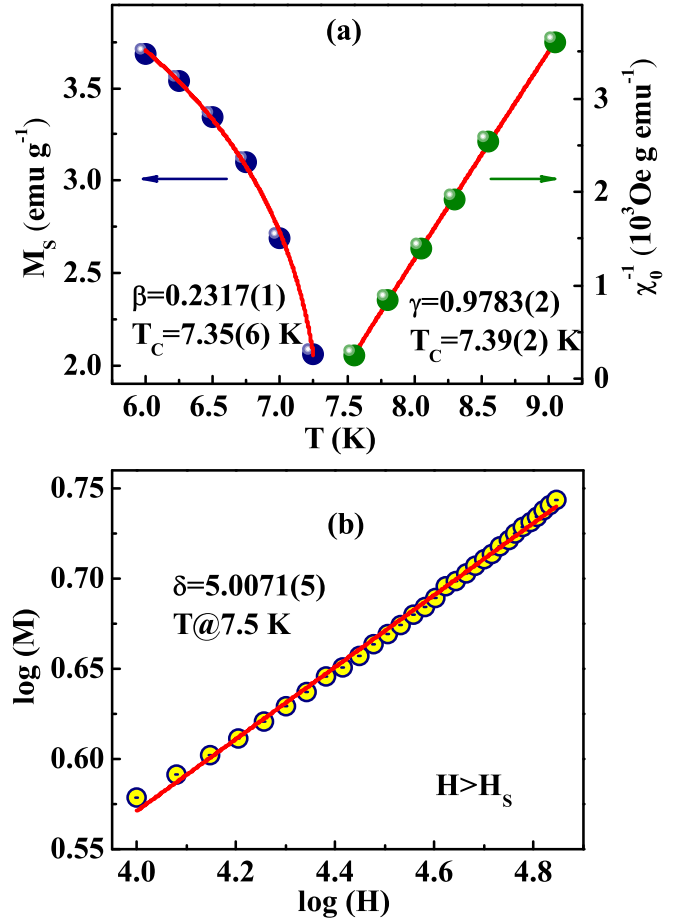


FIG. 8. (a)  $M_S$  (left) and  $\chi_0^{-1}$  (right) as a function of temperature for  $\text{La}_2\text{ZnIrO}_6$  (red curves are fitted); (b) isothermal  $M(H)$  at the critical temperature  $T_C$  on log-log scale (red line is fitted).

the renormalized field ( $h$ ) as  $h \equiv H\varepsilon^{-(\beta+\gamma)}$ , in the asymptotic critical region the scaling equations can be written as [30]

$$m = f_{\pm}(h), \quad (6)$$

where  $f_{\pm}$  are regular functions denoted as  $f_+$  for  $T > T_C$  and  $f_-$  for  $T < T_C$ . The scaling equation indicates that  $m$  vs  $h$  should form two independent universal branches for  $T > T_C$  and  $T < T_C$ , respectively. With the obtained critical exponents, the initial isothermal  $M(H)$  curves around the critical temperature are rescaled into  $m(h)$ . Figure 9(a) shows the scaling of  $M(H)$  curves [ $m(h)$ ] in the high field region ( $H > 10$  kOe), while Fig. 9(b) gives those on the log-log scale. In the high field region,  $m(h)$  curves above and below  $T_C$  collapse onto two independent branches, respectively.

However, if a field-induced phase transition occurs, the scaling becomes divergent at the boundary between the different phases due to the change of magnetic interaction [45]. Figure 10(a) shows the  $m(h)$  in low field region ( $H < 10$  kOe) on log-log scale at temperature range from 2 K to 8.5 K. The  $m(h)$  curves in the low field region do not collapse into a universal branch. The  $m(h)$  curves below the phase transition temperature are separated into three regions by two inflection points. These two inflection points are marked as  $H_{AF}^2$  and  $H_{CF}$ , respectively, as shown in Fig. 10(a). The three regions

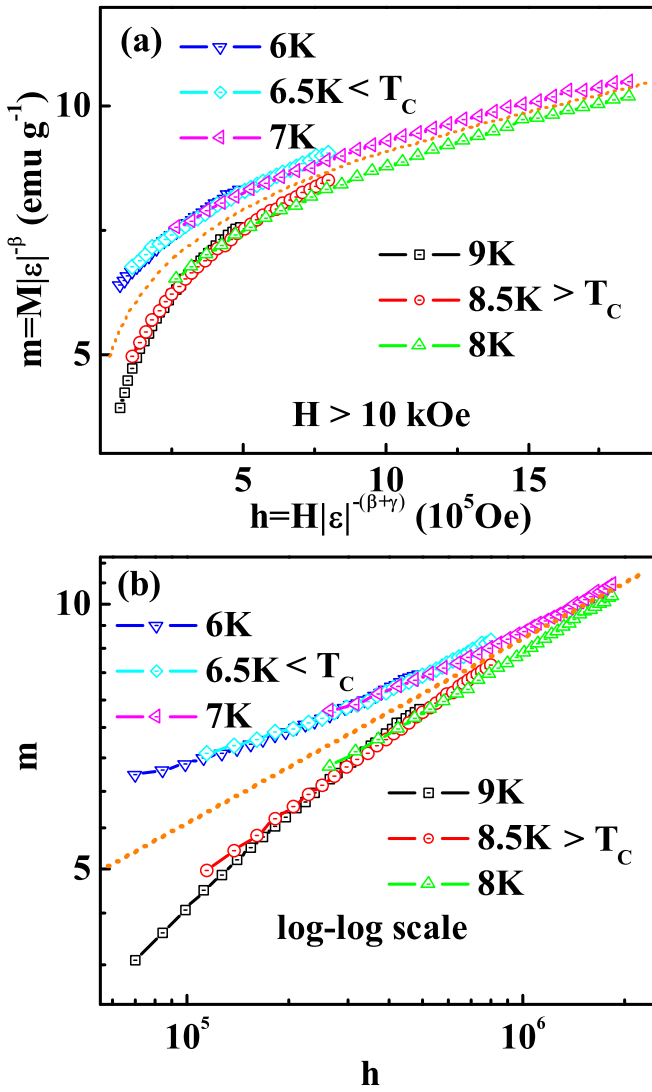


FIG. 9. (a) Scaling plot of the normalization magnetization  $m$  vs normalization field  $h$  around the critical temperature  $T_c$  in high field region; (b)  $m$  vs  $h$  curves on log-log scale.

are corresponding to the  $A$ -type AFM, canted-AFM, and FM phases, respectively. Thus the first inflection point marked as  $H_{AF}^2$  is the critical field from  $A$ -type AFM to canted-AFM state. The second one marked as  $H_{CF}$  corresponds to the critical field from canted-AFM phase to FM one.

In fact, the field-induced magnetic transition can be further confirmed by the Arrott plot [28]. Figure 10(b) shows the Arrott plot of  $M^2$  vs  $H/M$  curves in low field region on log-log scale. Also three regions are separated by two phase transitions, which are marked as  $H_{AF}^2$  and  $H_{CF}$ , respectively. It is known that the order of the phase transition can be determined by the slope ( $S$ ) of  $M^2$  vs  $H/M$  curve according to Banerjee's criterion. A negative slope suggests a first-order transition, while a positive slope implies a second-order one [46]. Therefore, based on Banerjee's criterion, the phase transition from AFM to FM is of the first-order type, because  $S$  changed from positive to negative. However, the magnetic transition from  $A$ -type AFM to canted AFM is not a first-order one, because  $S$  keeps positive in these two phases. The first-order phase transition is

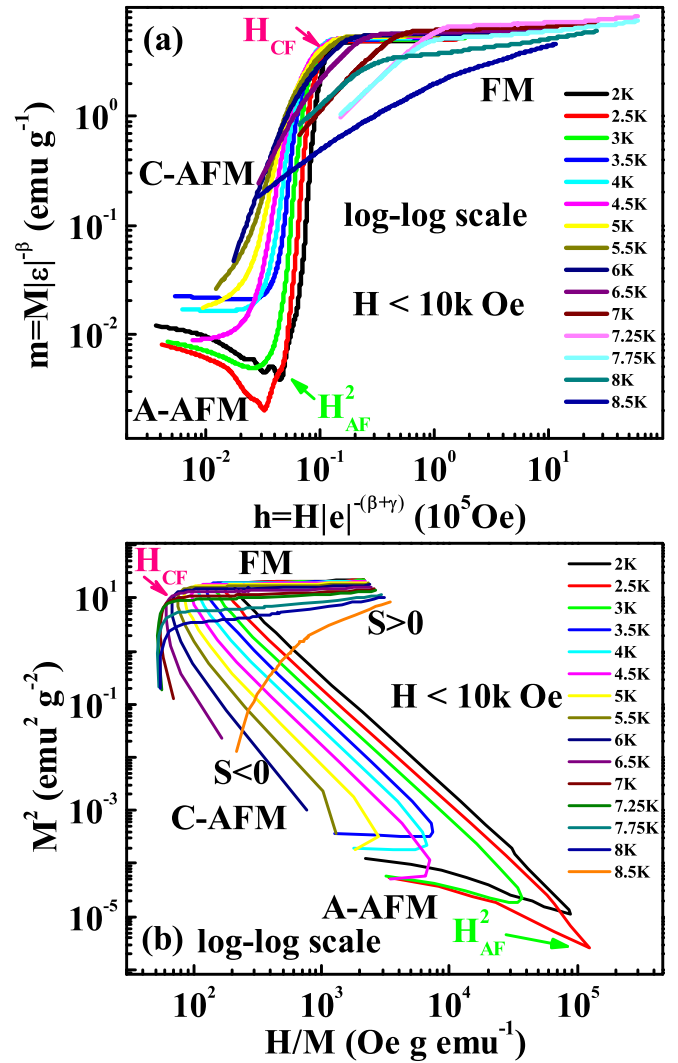


FIG. 10. (a)  $m$  vs  $h$  curves in low field region on log-log scale; (b)  $M^2$  vs  $H/M$  curves in low field region on log-log scale ( $H_{AF}^2$  denotes the critical field from  $A$ -type AFM to canted AFM;  $H_{CF}$  is the critical field from canted AFM to FM).

confirmed by the hysteresis on the  $M(H)$  (see Supplemental Material [27]), which is associated with the first-order phase transition [47].

Based on the scaling equation, the  $H$ - $T$  phase diagram of single crystal  $\text{La}_2\text{ZnIrO}_6$  with  $H//b$  is constructed, as shown in Fig. 11. The  $H$ - $T$  phase diagram presents multiple magnetic ordering phases. The critical behavior of  $\text{La}_2\text{ZnIrO}_6$  displays a field-induced tricritical phenomenon. In the low field region, the  $A$ -type AFM ordering ground state can be tuned into canted AFM by the external field. With further increase of the field, a phase transition from AFM to FM can be induced by the external field, which is of the first-order type. The boundary line of first-order phase transition terminates at the TCP ( $T_{Tr} \approx 8 \text{ K}$ ;  $H_{Tr} \approx 170 \text{ Oe}$ ). Meanwhile, from another view, the TCP locates among the boundaries between the AFM, FM, and PM phases. The field-induced magnetic phase transition results in the tricritical phenomenon in this system [47]. In fact, the tricritical phenomenon of  $\text{La}_2\text{ZnIrO}_6$  is very analogous to that in  $\text{USb}_2$ . In  $\text{USb}_2$ , a high magnetic field

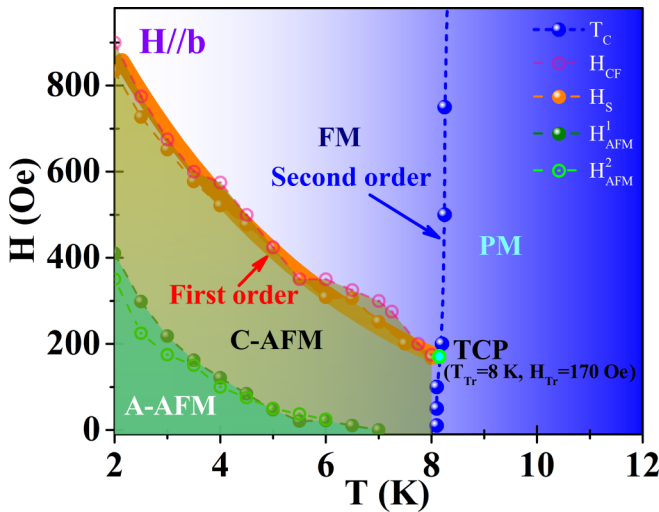


FIG. 11.  $H$ - $T$  phase diagram for single crystal  $\text{La}_2\text{ZnIrO}_6$  with  $H//b$  (A-AFM corresponds to the  $A$ -type antiferromagnetic ordering, C-AFM represents the canted antiferromagnetic ordering, FM denotes the ferromagnetic state, and PM means the paramagnetic phase).

induces a metamagnetic transition from AFM to ferrimagnetic (FIM) ordering, which is also of the first-order type [44]. Correspondingly, the transition changed from a second-order to first-order one at the TCP ( $T_{tr} \sim 145$  K and  $H_C \sim 52$  T)

in  $\text{USb}_2$ , which locates at the intersection point between the AFM, FIM, and PM phases [44].

#### IV. CONCLUSION

In summary, the magnetization of the double perovskite iridates  $\text{La}_2\text{ZnIrO}_6$  single crystal is systematically studied. The easy magnetic axis is along the  $ab$  plane according to the angle dependent isothermal  $M(H)$ ,  $M(T)$ , and  $M(\varphi)$  results, and is consistent with the  $A$ -type AFM characteristic in this system. Moreover, a first-order field-induced magnetic transition from AFM to FM state is found below  $T_N$ . The investigation of the critical behavior gives critical exponents  $\beta = 0.2317(1)$ ,  $\gamma = 0.9783(2)$ , and  $\delta = 5.0071(5)$ , which belong to the universality class of a tricritical mean-field model. The critical behavior of  $\text{La}_2\text{ZnIrO}_6$  suggests a field-induced tricritical phenomenon. Based on the scaling equations, we construct the  $H$ - $T$  phase diagram for single crystal  $\text{La}_2\text{ZnIrO}_6$  with  $H//b$ . The constructed  $H$ - $T$  phase diagram for  $\text{La}_2\text{ZnIrO}_6$  supports a tricritical point ( $T_{tr} \approx 8$  K;  $H_{tr} \approx 170$  Oe) existing at the intersection point between the AFM, FM, and PM phases.

#### ACKNOWLEDGMENTS

This work is supported by the National Key R&D Program of China (Grants No. 2017YFA0303201 and No. 2016YFA0401003) and the National Natural Science Foundation of China (Grants No. 11574322, No. U1732276, No. 51002060, No. 11574288, and No. 1147411).

- [1] B. J. Kim, H. Ohsumi, T. Komesu, S. Sakai, T. Morita, H. Takagi, and T. Arima, *Science* **323**, 1329 (2009).
- [2] G. Cao, J. Terzic, H. D. Zhao, H. Zheng, L. E. De Long, and P. S. Riseborough, *Phys. Rev. Lett.* **120**, 017201 (2018).
- [3] B. J. Kim, H. Jin, S. J. Moon, J. Y. Kim, B. G. Park, C. S. Leem, J. Yu, T. W. Noh, C. Kim, S. J. Oh, J. H. Park, V. Durairaj, G. Cao, and E. Rotenberg, *Phys. Rev. Lett.* **101**, 076402 (2008).
- [4] L. Zhao, D. H. Torchinsky, H. Chu, V. Ivanov, R. Lifshitz R. Flint, T. Qi, G. Cao, and D. Hsieh, *Nat. Phys.* **12**, 32 (2016).
- [5] L. Balents, *Nature (London)* **464**, 199 (2010).
- [6] Y. Machida, S. Nakatsuji, S. Onoda, T. Tayama, and T. Sakakibara, *Nature (London)* **463**, 210 (2010).
- [7] S. Nakatsuji, Y. Machida, Y. Maeno, T. Tayama, T. Sakakibara, J. van Duijn, L. Balicas, J. N. Millican, R. T. Macaluso, and J. Y. Chan, *Phys. Rev. Lett.* **96**, 087204 (2006).
- [8] Z. Tian, Y. Kohama, T. Tomita, H. Ishizuka, T. Hsieh, J. Ishikawa, K. Kindo, L. Balents, and S. Nakatsuji, *Nat. Phys.* **12**, 134 (2015).
- [9] K. Ueda, J. Fujioka, B. J. Yang, J. Shiozaki, A. Tsukazaki, S. Nakamura, S. Awaji, N. Nagaosa, and Y. Tokura, *Phys. Rev. Lett.* **115**, 056402 (2015).
- [10] D. Pesin and L. Balents, *Nat. Phys.* **6**, 376 (2010).
- [11] M. Nakayama, T. Kondo, Z. Tian, J. J. Ishikawa, M. Halim, C. Bareille, W. Malaeb, K. Kuroda, T. Tomita, S. Ideta, K. Tanaka, M. Matsunami, S. Kimura, N. Inami, K. Ono, H. Kumigashira, L. Balents, S. Nakatsuji, and S. Shin, *Phys. Rev. Lett.* **117**, 056403 (2016).
- [12] H. B. Zhang, K. Haule, and D. Vanderbilt, *Phys. Rev. Lett.* **118**, 026404 (2017).
- [13] X. Wan, A. M. Turner, A. Vishwanath, and S. Y. Savrasov, *Phys. Rev. B* **83**, 205101 (2011).
- [14] W. W. Krempa, G. Chen, Y. B. Kim, and L. Balents, *Annu. Rev. Condens. Matter Phys.* **5**, 57 (2014).
- [15] S. Vasala and M. Karppinen, *Prog. Solid State Chem.* **43**, 1 (2015).
- [16] R. C. Currie, J. F. Vente, E. Frikkie, and D. J. W. Ijdo, *J. Solid State Chem.* **116**, 199 (1995).
- [17] K. Manna, R. Sarkar, S. Fuchs, Y. A. Onykieenko, A. K. Bera, G. A. Cansever, S. Kamusella, A. Maljuk, C. G. F. Blum, L. T. Corredor, A. U. B. Wolter, S. M. Yusuf, M. Frontzek, L. Keller, M. Iakovleva, E. Vavilova, H. J. Grafe, V. Kataev, H. H. Klauss, D. S. Inosov, S. Wurmehl, and B. Büchner, *Phys. Rev. B* **94**, 144437 (2016).
- [18] S. Bhowal and I. Dasgupta, *Phys. Rev. B* **97**, 024406 (2018).
- [19] F. Hammerath, R. Sarkar, S. Kamusella, C. Baines, H.-H. Klauss, T. Dey, A. Maljuk, S. Gaß, A. U. B. Wolter, H.-J. Grafe, S. Wurmehl, and B. Büchner, *Phys. Rev. B* **96**, 165108 (2017).
- [20] N. Narayanan, D. Mikhailova, A. Senyshyn, D. M. Trots, R. Laskowski, P. Blaha, K. Schwarz, H. Fuess, and H. Ehrenberg, *Phys. Rev. B* **82**, 024403 (2010).
- [21] M. Vogl, L. T. Corredor, T. Dey, R. Morrow, F. Scaravaggi, A. U. B. Wolter, S. Aswartham, S. Wurmehl, and B. Büchner, *Phys. Rev. B* **97**, 035155 (2018).
- [22] M. P. Ghimire, L. H. Wu, and X. Hu, *Phys. Rev. B* **93**, 134421 (2016).

- [23] G. Cao, A. Subedi, S. Calder, J. Q. Yan, J. Yi, Z. Gai, L. Poudel, D. J. Singh, M. D. Lumsden, A. D. Christianson, B. C. Sales, and D. Mandrus, *Phys. Rev. B* **87**, 155136 (2013).
- [24] A. A. Aczel, A. M. Cook, T. J. Williams, S. Calder, A. D. Christianson, G.-X. Cao, D. Mandrus, Y.-B. Kim, and A. Paramekanti, *Phys. Rev. B* **93**, 214426 (2016).
- [25] A. M. Cook, S. Matern, C. Hickey, A. A. Aczel, and A. Paramekanti, *Phys. Rev. B* **92**, 020417(R) (2015).
- [26] W. K. Zhu, C. K. Lu, W. Tong, J. M. Wang, H. D. Zhou, and S. X. Zhang, *Phys. Rev. B* **91**, 144408 (2015).
- [27] See Supplemental Material at <http://link.aps.org/supplemental/10.1103/PhysRevB.98.054403> for the characterization of the single crystal, the determination of the crystal orientations, and the hysteresis on  $M(H)$  curve.
- [28] A. Arrott, *Phys. Rev.* **108**, 1394 (1957).
- [29] A. Arrott and J. Noakes, *Phys. Rev. Lett.* **19**, 786 (1967).
- [30] H. E. Stanley, *Introduction to Phase Transitions and Critical Phenomena* (Oxford University Press, London, 1971).
- [31] M. E. Fisher, *Rev. Mod. Phys.* **46**, 597 (1974).
- [32] K. Huang, *Statistical Mechanics*, 2nd ed. (Wiley, New York, 1987).
- [33] S. N. Kaul, *J. Magn. Magn. Mater.* **53**, 5 (1985).
- [34] J. Y. Fan, L. S. Ling, B. Hong, L. Zhang, L. Pi, and Y. H. Zhang, *Phys. Rev. B* **81**, 144426 (2010).
- [35] L. Zhang, B. S. Wang, Y. P. Sun, P. Tong, J. Y. Fan, C. J. Zhang, L. Pi, and Y. H. Zhang, *Phys. Rev. B* **85**, 104419 (2012).
- [36] L. P. Kadanoff, *Physics* **2**, 263 (1966).
- [37] V. Taufour, D. Aoki, G. Knebel, and J. Flouquet, *Phys. Rev. Lett.* **105**, 217201 (2010).
- [38] D. Kim, B. Revaz, B. L. Zink, F. Hellman, J. J. Rhyne, and J. F. Mitchell, *Phys. Rev. Lett.* **89**, 227202 (2002).
- [39] M. H. Phan, V. Franco, N. Bingham, H. Srikanth, N. Hur, and S. Yu, *J. Alloys Compd.* **508**, 238 (2010).
- [40] A. Bauer, M. Garst, and C. Pfleiderer, *Phys. Rev. Lett.* **110**, 177207 (2013).
- [41] L. Zhang, D. Menzel, C. M. Jin, H. F. Du, M. Ge, C. J. Zhang, L. Pi, M. L. Tian, and Y. H. Zhang, *Phys. Rev. B* **91**, 024403 (2015).
- [42] A. E. Petrova, V. N. Krasnorussky, J. Sarrao, and S. M. Stishov, *Phys. Rev. B* **73**, 052409 (2006).
- [43] M. Otero-Leal, F. Rivadulla, S. S. Saxena, K. Ahilan, and J. Rivas, *Phys. Rev. B* **79**, 060401 (2009).
- [44] R. L. Stillwell, I. L. Liu, N. Harrison, M. Jaime, J. R. Jeffries, and N. P. Butch, *Phys. Rev. B* **95**, 014414 (2017).
- [45] H. Han, L. Zhang, D. Sapkota, N. Hao, L. Ling, H. Du, L. Pi, C. Zhang, D. G. Mandrus, and Y. Zhang, *Phys. Rev. B* **96**, 094439 (2017).
- [46] B. K. Banerjee, *Phys. Lett.* **12**, 16 (1964).
- [47] E. Strykowski and N. Giordano, *Adv. Phys.* **26**, 487 (1977).